# Quantum chemical insight properties of glyphosine(N, N-Bis (phosphonomethyl) glycine) – a combined hf and density functional study

A. Gokila[a,*], S. Ayyappan[b]
[a]Department of Science and Humanities, Sri Eshwar College of
Engineering,Kinathukkadavu, Tamil Nadu 641202, India
[b]Department of Physics, Government College of Technology, Coimbatore, Tamil
Nadu 64101, India

The ab initio HF and Density Functional (DFT / B3LYP) method with a 6-31G(d, p) basis
was used to declare a geometric structure and vibrational wave ranges of the glyphosine
(GPS) (N, N-Bis (phosphonomethyl) glycine). HF and DFT calculations have optimized
geometric hops. The B3LYP method, basis set on a 6-31 G (d, p), is the best level in
theory for repeating constructive wave numbers.Density functional theory was used to
explore the first hyperpolarizability ($\beta$) of the GPS. The results of the computations also
indicate that the fragment GPS could be analyzed with Natural Bond Orbital (NBO). The
FT-IR and FT-Raman theoretical spectra were constructed for the title component. The
prospective, absolute and partial molecular electrostatic density (TDOS, PDOS) was
evaluated for the GPS. The established energy from HOMO and LUMO shows that the
charge is transferred in the fragment.

## 1. Introduction

The natural phenolic composite glyphosine (N, N-Bis (phosphonomethyl), which is most
commonly found in rice bran, wheat, barley, tomatoes and toasted coffee.Glyphosine is a control
mechanism for plant growth that is embedded in chlorosis in leaves of many plant varieties [1,2].
The authors observed that compound glyphosine increased the production of insulin and prevented
diabetes in mice from developing type 1 diabetes inheritably. The same thing happened in human
cells also [3]. Eight sugarcane growth were cultivated with addition of unusual types of glyphosine
the consequences of sucrose content [4].A fish exposed to plagiarist glyphosine extend digestive
disorders reminiscent of coeliac disease. Celiac disease includes inequity of intestinal bacteria that
are clearly demonstrated by the known effects of plagiaristic glyphosine on intestinal bacteria
[5].However, a recent paper suggested that the plagiatricglyphosine may be a major contributor to
fatness, autism and many other disorders in the United States such as Alzheimer's, Parkinson's,
infertility, depression and cancer [6]. The 5-enolpyruvyl shikimic acid-3-phosphate synthesis
(EPSP synthesis) was suppressed by Glyphosine Plagiary, the rate limiting stage in the aromatized
amino acid syntheses of bacteria, archaea and plants [7,8]. This method is exclusive to the
plagiaristic glyphosine of all herbicides that emerge. Humans do not have this path, so we depend
on our food we eat and the microbes we burn to provide the nutrients we need. Plagiary
glyphosine, an antimicrobial patent [9].A recent study in carnivorous fish exposed to glyphosine
plagiarism showed significant adverse effects throughout the digestive system [10]. Several more
features, including iron and cobalt, of Glyphosine plagiarism and contact with cytochrome
enzymes, which play a significant part in the body, are also detrimental to human health. Protease,
lipase and amylase production in the stomach and intestine have all been reduced following
exposure to plagiarist glyphosine. The authors have discussed 'mucosal fold destruction and
misunderstanding of the intestinal system,' and the over-secretion of mucine over the food tract.
The characteristics of this disease are highly evocative. Gluten peptides are hydrophobic in wheat
and therefore not prepared for gastric, pancreatic and intestinal protease degradation [11]. The

---

* Corresponding author: ayyappan@gct.ac.in

evidence of this effect on fish therefore suggests that glyphosine plagiarism that prevents the breakdown of multifaceted proteins in the stomach by leaving large amounts of wheat in the gut which will then cause autoimmune reactions that lead to the small intestine imperfections which are characterized by the glyphosine plagiarism and the disease of these fish. Plagiaristic sugar cane can explain the recent inflammation of the kidney [12].Ingeneral; the dry-weight accumulation of glyphosine was the most inhibitory and caused the greatest embarrassment. In light-grown and dark-grown soybean axes, glyphosine significantly increased the effect of extractable PAL (phenylalanine Ammonia-lyase) in less than glyphosate [13].The GPS is used for chickens and the concentrated weight and important mineral levels are determined in the bones of the tibiotrate. In the sister chromatic exchange of human lymphocytes a moderate stimulant result has been found to be a marketable drug containing the glyphosineisopropsyleamine salt [14].

Raman spectra and the calculated results without fluorescence can help in defining vibration modes and the connecting and structural attributes of organic composite molecular systems. In order to explain the details on charge transfer inside the fragment, both IR and Raman spectroscopy have been used in Homo, Lumo and hyperpolarizability studies. The present work deals with the estimation of HF and density theoretical function (DFT) and the vibrational spectral analysis of the amino and carboxylic acid Glyphosine (GPS). This work supports the diagnosis, treatment and efficiency of different diseases such as cancer in human beings and plant species.

## 2. Experimental details

Glyphosine (N, N-Bis (phosphonomethyl) glycine) was purchased in and used without additional purification from Sigma – Aldrich Chemical Company (USA), which was asserted to be purified at more than 98 percent. In the region of 400 – 4000 cm$^{-1}$ the IFS 66V spectrophotometer with KBr pellet technique recorded the FT-IR spectrum of this composite. Spectrums with a scanning velocity of 30 cm$^{-1}$ min$^{-1}$ and with a spectral resolution of 2.0 cm$^{-1}$, were found at room temperature. The Laser-Raman GPS spectrum of a Brucker model IFS 66 V spectrophotometer with FRA 106 FT-Raman accessory was recorded using 1064 nm Nd : YAG laser as the exciting wavelength of around 400–4000 cm$^{-1}$. In Figures.1-4, the reported FT-IR and Laser-Raman spectrums with IR and Raman theoretical spectra are shown. Spectral measurements have been conducted at Government College of Technology, Coimbatore and BharathiarUniversity,Tamilnadu, India.

## 3.Computational details

Based on the GAUSSIAN 09w [15] package program for Intel i7 personal computer calculations of ab initio HF and DFT (B3LYP); geometry restriction is not needed here [16]. First, the Glyphosine model (GPS) has been designed with complete energy surface relaxation at HF/6-31 G (d, p) and the resulting geometries have been used as inputs for further DFT (B3LYP) calculations. For the measurement of vibrational occurrences at the DFT level, optimized structural hops were used to reduce all stationary points. The vibrational frequency assignments were accomplished with high precision with the use of GAUSSVIEW [17] and VEDA [18] along with related fragments available. In order to enhance the treatment of the hydroxyl groups, polarization functions were applied.

## 4. Hyperpolarizability

The first glyphosine hyper-polarisability(β0) and its related (β, α0 and Δα) were calculated based on the finite field method using HF/6-31 G (d, p) bases. The hyper-polarisability of Kleinman symmetry [19] is a third-grade tensor that can be represented by a matrix of 3×3×3 And can be reduced by as many as 10 components, with 27 components of the 3-dimensional matrix.

The lower part of the 3×3×3 matrixes is obviously a tetrahedral. The mechanisms of β are different from the energy expansion coefficients in the outer electrical field of the Taylor series.

$$E = E^0 - \mu_\alpha F_\alpha - 1/2\alpha_{\alpha\beta}F_\alpha F_\beta - 1/6\beta_{\alpha\beta\gamma}F_\alpha F_\beta F_\gamma + \cdot \tag{1}$$

In equation (1), where $E^0$ is the energy of non-perturbed fragments, $F_\alpha$ is the ground at the origins $\mu_\alpha$, $\alpha_{\alpha\beta}$ and $\beta_{\alpha\beta\gamma}$, respectively, are the parts of the dipole moment, polarizability and the first hyper-polarizability. The total static μ, the mean $\alpha_0$ polarization, the mean first β0 hyperpolarisability for the Cartesian coordinate are described by

$$\mu = (\mu^2_x + \mu^2_y + \mu^2_z)^{1/2} \tag{2}$$

$$\alpha_0 = \frac{\alpha_{xx} + \alpha_{yy} + \alpha_{zz}}{3} \tag{3}$$

$$\alpha = 2^{-1/2}[(\alpha_{xx} - \alpha_{yy})^2 + (\alpha_{yy} - \alpha_{zz})^2 + (\alpha_{zz} - \alpha_{xx})^2 + 6\alpha^2 xx]^{1/2} \tag{4}$$

$$\beta_0 = (\beta^2_x + \beta^2_y + \beta^2_z)^{1/2} \tag{5}$$

$$\beta_x = \beta_{xxx} + \beta_{xyy} + \beta_{xzz} \tag{6}$$

$$\beta_y = \beta_{yyy} + \beta_{xxy} + \beta_{yzz} \tag{7}$$

$$\beta_z = \beta_{zzz} + \beta_{xxz} + \beta_{yyz} \tag{8}$$

The GPS first hyperpolarizability for HF/6-31 G (d, p) system has been achieved at $6.159X\ 10^{-30}$esu, as shown in Table 1 and Table 2.

*Table 1.The ab initio calculated electric dipole moments m (Debye) and dipole moment components for Glyphosine.*

|  | HF /6-31G(d) |
|---|---|
| $\mu_x$ | 1.3795 |
| $\mu_y$ | -1.6297 |
| $\mu_z$ | -9.4553 |
| $\mu$ | 9.6934 |

*Table 2. Calculated all β components and $\beta_{tot}(\times 10^{-30})$ value of Glyphosine.*

|  | HF /6-31G(d) |
|---|---|
| $\beta_{xxx}$ | -172.7986 |
| $\beta_{xxy}$ | -198.2945 |
| $\beta_{xyy}$ | -115.1295 |
| $\beta_{yyy}$ | -423.2585 |
| $\beta_{xxz}$ | -94.3689 |
| $\beta_{xyz}$ | 52.0453 |
| $\beta_{yyz}$ | 44.7698 |
| $\beta_{xzz}$ | 33.6780 |
| $\beta_{yzz}$ | 68.7228 |
| $\beta_{zzz}$ | 68.7228 |
| $\beta_{total(esu)}$ | $6.15906 \times 10^{-30}$ |

## 5. Result and discussion

### 5.1. Geometric structure

The optimized GPS monomer hops and dimer hops worked out by ab initio HF and DFT (B3LYP) level through the basis set of 6-31 G (d, p) are listed in (Table 3a) respectively and shown in figure 5 and 6. The bond lengths of C-N is 1.469Å for the amine group and 1.472Å for aziridine group the optimized single bond length range of C-N were 1.4504 – 1.465 Å by B3LYP/6-31G (d, p) method. As soon as the addition of the substituent groups (hydroxyl group) roots slightdisparities between them. The length of the bond of C7-C10 for the title fragment has been 1.5161 Å and 1.5237 Å, formed by HF and abintio DFT theory, on a base set of 6-31 G (d, p). Several authors [20] have clarified the increase in bond length of the C-H bond as a result of a change in carbon atom charge allocation. The exchange may be of the form of withdrawal (F, Cl, Br, N, etc.) or an electron form of donation. The strongly attracted carbon atom of the hydrogen cloud's valence electrons increases the constant CH force and reduces the bond length by the introduction of a number of substitutes. The opposite is valid for electron donor groups substitution. The real shift in the length of the C- H bond will be determined by the combined effect of mensomer-inductive contact and the electrical dipole field of the polar replacement. In this analysis, the bonding lengths of 1.0832, 1.0882 and 1.0798 Å have been measured as C2-H3, C7-H8, C7-H9, and C7-H10, but the length of the bond of C2-H4 is increased by about 0.01 Å because of phosphorous atom contact in this GPS community.
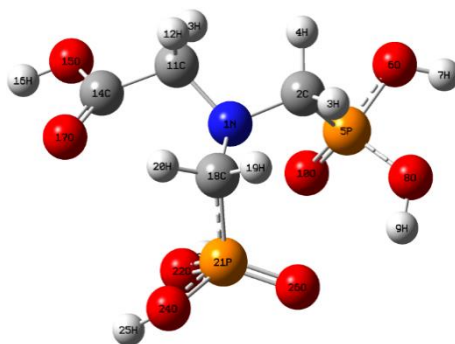


*Fig. 5. Geometrical structure of Glyphosine.*

The hops obtained using the B3LYP method with pole separated base sets are roughly the same as those tentatively observed. The defined bond length and bond angles are very close to the provisional values at all rates listed here. Interestingly enough, it has been drawn up using the HF method that both the P-O bond lengths between 1.4509 -1.5975, and 1.4791-1.6439 Å were formed using DFT Theory. The lengths of the P-O bond differ. The reversal between the single electron pair of the oxygen atom and the electron pair of the nitrogen atom can be due to this effect. For the monomer of the fragment named "DFT/ B3LYP/6-31G(d, p)" the bond longitude of O41-H42 and O15-H16 is 1.0042 Å. The fragments are stabilized by the intermolecular O – H — O bonds' endless chain. B3LYP/6-31 G (d, p) method is used to build computational dimer hops (intermolecular hydrogen bonding). From the (Table 3b), theoretical values, it can be found that most of the optimized bond lengths O41-H42--O17 and O15-H16---O43 are close to the bonding length value of 1,657 Å and the bond angle of corresponding value is 179.6 compared to the bond angles and length of B3LYP/6-31 G (d, p).
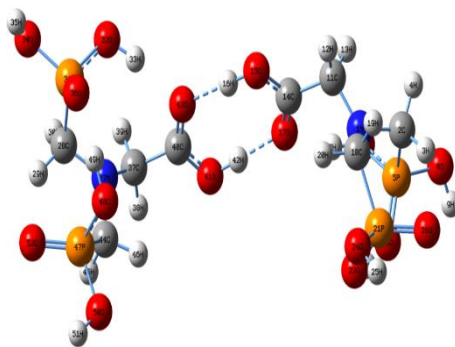
*Fig. 6.Geometrical structure of dimer of Glyphosine.*

*Table 3a.Geometrical parameters optimized in (FA), bond length (A°), bond angle (∘)
and dihedral angle (°).*

| Parameters | HF 6-31G(d,p) | B3LYP 6-31G(d,p) | Parameters | HF 6-31G(d,p) | B3LYP 6-31G(d,p) |
|---|---|---|---|---|---|
| **Bond length (Aᵒ)** | | | | | |
| N1-C2 | 1.4504 | 1.453 | N1-C7-H8 | 112.2 | 110.5 |
| N1-C7 | 1.4545 | 1.4643 | N1-C7-H9 | 108.9 | 109.6 |
| N1-C12 | 1.465 | 1.4696 | N1-C7-C10 | 110.7 | 107.5 |
| C2-H3 | 1.0832 | 1.0921 | H8-C7-H9 | 109.4 | 108.6 |
| C2-H4 | 1.0904 | 1.1006 | H8-C7-C10 | 107.6 | 124.1 |
| C2-P5 | 1.8086 | 1.8303 | H9-C7-C10 | 108.0 | 111.5 |
| P5-O6 | 1.4509 | 1.4791 | C7-C10-O11 | 123.7 | 124.4 |
| P5-O19 | 1.5975 | 1.6439 | 7C-C10-O23 | 112.3 | 112.1 |
| P5-O21 | 1.5794 | 1.6117 | O11-C10-O23 | 124.0 | 111.0 |
| C7-H8 | 1.0882 | 1.0992 | N1-C12-H13 | 112.3 | 109.1 |
| C7-H9 | 1.0798 | 1.0899 | N1-C12-H14 | 110.9 | 107.4 |
| C7-C10 | 1.5161 | 1.5237 | N1-C12-P15 | 108.7 | 108.7 |
| C10-O11 | 1.182 | 1.2039 | H13-C12-H14 | 107.2 | 108.4 |
| C10-O23 | 1.3178 | 1.3425 | H13-C12-P15 | 109.7 | 116.4 |
| C12-H13 | 1.0849 | 1.0938 | H14-C12-P15 | 107.9 | 102.1 |
| C12-H14 | 1.0837 | 1.0935 | C12-P15-O16 | 115.6 | 103.8 |
| C12-P15 | 1.8099 | 1.835 | C12-P15-O17 | 102.7 | 114.8 |
| P15-O16 | 1.451 | 1.4816 | C12-P15-O25 | 104.5 | 116.4 |
| P15-O17 | 1.5811 | 1.6172 | O16-P15-O17 | 114.7 | 101.2 |
| P15-O25 | 1.5792 | 1.6104 | O16-P15-O25 | 115.4 | 111.3 |
| O17-H18 | 0.9438 | 0.9644 | O17-P15-O25 | 102.2 | 109.4 |
| O19-H20 | 0.9455 | 0.9667 | P15-O17-H18 | 114.2 | 114.5 |
| O21-H22 | 0.9443 | 0.9651 | P5-O19-H20 | 112.2 | 107.2 |
| O23-H24 | 0.9465 | 0.9696 | P5-O21-H22 | 115.3 | 113.4 |
| O25-H26 | 0.9486 | 0.9745 | C10-O23-H24 | 108.9 | 110.5 |
| **Bond angle (ᵒ)** | | | P15-O25-H26 | 114.7 | 109.6 |
| C2-N1-C7 | 114.2 | 114.7 | N1-C7-H8 | 112.2 | 107.5 |
| C2-N1C12 | 115.1 | 116.2 | N1-C7-H9 | 108.9 | 108.6 |

| Parameters | HF 6-31G(d,p) | B3LYP 6-31G(d,p) | Parameters | HF 6-31G(d,p) | B3LYP 6-31G(d,p) |
|---|---|---|---|---|---|
| Bond length (A°) | | | | | |
| C7-N1-C12 | 113.9 | 114.6 | | | |
| N1-C2-H3 | 110.0 | 110.2 | | | |
| N1-C2-H4 | 113.3 | 113.7 | | | |
| N1-C2-P5 | 114.9 | 114.4 | | | |
| H3-C2-H4 | 106.7 | 106.7 | | | |
| H3-C2-P5 | 103.9 | 104.1 | | | |
| H4-C2-P5 | 107.4 | 107.0 | | | |
| C2-P5-O6 | 115.6 | 116.5 | | | |
| C2-P5-O19 | 104.4 | 104.8 | | | |
| C2-P5-O21 | 104.1 | 101.7 | | | |
| O6-P5-O19 | 111.9 | 111.7 | | | |
| C6-P5-O21 | 114.5 | 117.0 | | | |
| O19-P5-O21 | 105.1 | 103.5 | | | |

*Table 3a. (Contd.)*

| Parameters | HF 6-31G(d,p) | B3LYP 6-31G(d,p) | Parameters | HF 6-31G(d,p) | B3LYP 6-31G(d,p) |
|---|---|---|---|---|---|
| Dihedral angle (°) | | | | | |
| C7-N1-C2-H3 | 155.2 | 153.9 | O8-P5-O6-H7 | -77.2 | -125.1 |
| C7-N1-C2-H4 | 35.9 | 34.2 | O8-P5-O6-H7 | 173.8 | 2.0 |
| C7-N1-C2-P5 | -88.0 | -89.2 | H12-C11-C14-O15 | 12.2 | 70.0 |
| C12-N1-C2-H3 | 20.8 | 16.5 | H12-C11-C14-O17 | -170.2 | -14.4 |
| C12-N1-C2-H4 | -98.5 | -103.2 | H13-C11-C14-O15 | -102.7 | 167.2 |
| C12-N1-C2-P5 | 137.6 | 133.4 | H13-C11-C14-O17 | 74.9 | -132.8 |
| C2-N1-C7-H8 | -79.6 | -78.0 | C11-C14-O15-H16 | 177.1 | 48.7 |
| C2-N1-C7-H9 | 41.7 | 43.2 | O17-C14-O15-H16 | -0.6 | 164.2 |
| C2-N1-C7-C10 | 160.2 | 162.0 | N1-C18-P21-O24 | -163.8 | -14.2 |
| C12-N1-C7-H8 | 55.4 | 60.0 | N1-C18-P21-O26 | 73.8 | -71.9 |
| C12-N1-C7-H9 | 176.6 | -178.8 | H19-C18-P21-O24 | 70.5 | 162.3 |
| C12-N1-C7-C10 | -64.8 | -59.9 | H19-C18-P21-O26 | -52.0 | 57.4 |
| C2-N1-C12-H13 | 14.4 | 10.5 | H20-C18-P21-O24 | -44.2 | 165.6 |
| C2-N1-C12-H14 | 134.4 | 130.7 | H20-C18-P21-O26 | -166.7 | 39.9 |
| C2-N1-C12-P15 | -107.1 | -109.9 | N1-C18-O22-O23 | 19.2 | -65.1 |
| C7-N1-C12-H13 | -120.1 | -126.9 | H19-C18-O22-O23 | -114.7 | 49.2 |
| C7-N1-C12-H14 | -0.2 | -6.7 | H20-C18-O22-O23 | 127.6 | -76.6 |
| C7-N1-C12-P15 | 118.4 | 112.7 | O24-P21-O22-O23 | -173.5 | 178.5 |
| N1-C2-P5-O6 | -178.2 | -175.6 | O26-P21-O22-O23 | -47.3 | 145.3 |
| N1-C2-P5-O19 | -54.7 | -51.5 | C18-P21-O24-H25 | -147.2 | 18.5 |
| N1-C2-P5-O21 | 55.3 | 56.0 | O22-P21-O24-H25 | 103.0 | -107.8 |

| Parameters | HF 6-31G(d,p) | B3LYP 6-31G(d,p) | Parameters | HF 6-31G(d,p) | B3LYP 6-31G(d,p) |
|---|---|---|---|---|---|
| **Dihedral angle ($^o$)** | | | | | |
| H3-C2-P5-O6 | -57.9 | -55.3 | O26-P21-O24-H25 | -24.8 | -68.0 |
| H3-C2-P5-O19 | 65.5 | 68.8 | H4-C2-P5-O10 | 174.2 | -70.9 |
| H3-C2-P5-O21 | 175.5 | 176.3 | C2-P5-O6-H7 | -77.2 | -125.1 |
| H4-C2-P5-O6 | 54.9 | 57.5 | O8-P5-O6-H7 | 173.8 | 2.0 |
| H4-C2-P5-O19 | 178.3 | -178.4 | O10-P5-O6-H7 | 49.4 | 128.7 |
| H4-C2-P5-O21 | -71.7 | -70.9 | C2-P5-O8-H9 | 142.6 | 178.1 |
| C2-P5-O19-H20 | -133.9 | -125.1 | O6-P5-O8-H9 | -107.5 | 50.0 |
| O6-P5-O19-H20 | -8.1 | 2.0 | N1-C11-C14-O15 | 137.2 | -73.3 |
| O21-P5-O19-H20 | 116.8 | 128.7 | N1-C11-C14-O17 | -45.2 | 108.5 |
| C2-P5-O21-H22 | 157.5 | 178.1 | H12-C11-C14-O15 | 12.2 | -70.0 |
| O6-P5-O21-H22 | 30.2 | 50.0 | H12-C11-C14-O17 | -170.2 | -14.4 |
| O19-P5-O21-H22 | -93.0 | -73.3 | H13-C11-C14-O15 | -102.7 | 167.2 |
| N1-C7-C10-O11 | 110.6 | 108.5 | H13-C11-C14-O17 | 74.9 | -132.8 |
| N1-C7-C10-O23 | -69.4 | -70.9 | C11-C14-O15-H16 | 177.1 | 48.7 |

*Table 3b. Intermolecular hydrogen bonding parameters based on B3LYP/6-31G (d,p) method.*

| O41-H42….O17 | O41-H42 | H42….O17 | O43….O17 | O41-H42….O17 |
|---|---|---|---|---|
| | 1.0042 | 1.657 | 3.283 | 179.6 |
| O15— H16…..O43 | O15—H16 | H16…..O43 | O23…..O39 | O23—H22…..O39 |
| | 1.0042 | 1.656 | 3.283 | 179.6 |

### 5.2.1. Vibrational spectral analysis

The vibration study of GPS has been performed on the basis of methoxy, propenoic acid, hydroxy and phenyl ring mode characteristic vibrations. HF and density functional theory (B3LYP and BLYP), with a 6-31 G (d, p) base set, have been applied to theoretic calculations. The fragment of title is not planar and forms part of the category of C1 points. No corresponding distribution will exist for C1 symmetry. Three specific scaling factors were found in our research. HF/6-31G (d, p): 0.9026, BLYP/6-31G (d, p):0.9923 and B3LYP/6-31G (d, p): 0.9608[21,22] as shown in (Table 4).
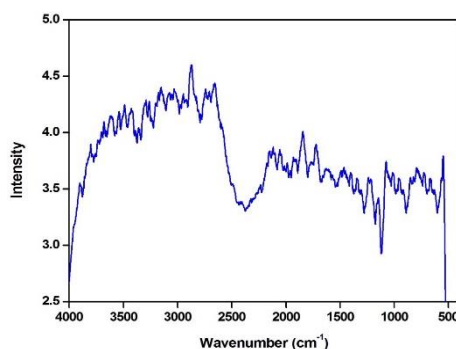


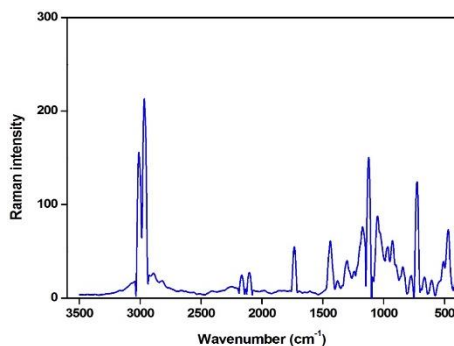*Fig. 1. Experimental FT IR spectrum of Glyphosine.*

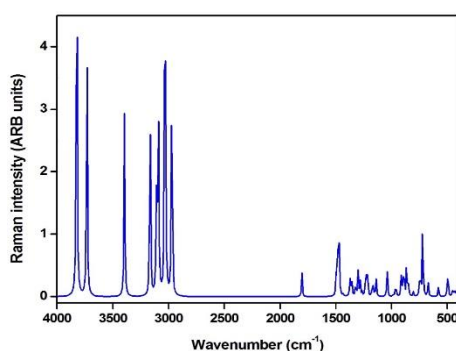*Fig. 2.Experimental FT Raman spectrum of Glyphosine.*
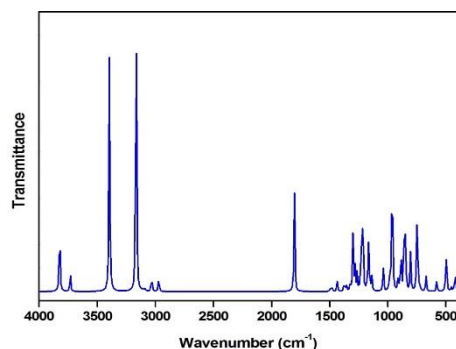


*Fig. 3. Computed FT-IR spectra of Glyphosine.*



*Fig. 4.Computed FT-Raman spectra of Glphosine.*

### 5.2.2. O-H vibrations

The O-H group produces three vibrations (spreading, winding and tearing out of the plane). The O-H group vibrations are most likely to be environmentally sensitive, displaying significant differences in the hydrogen-linked species' spectrum. In the area of about 3580-3650 cm^{-1}, hydroxy stretching vibrations are normally [23] observed. The frequency of O-H vibration in the gas phase has been shown to be 3657 cm[-1][24]. Similarly, the O-H stretching vibrations have been assigned to our FT-IR 3679, 3615 and 3490 cm^{-1} band. Based on the literature data forecast, the harmonic approximation of the vibration intramolecular hydrogen bonds in the atomic group is a slight deviation.The in-ground frequency of the O-H bending in general is 1150-1250 cm^{-1} and, unlike the expanding and out of-ground bending frequencies of the hydrogen bond, it isn't affected much [25]. In the flat winding vibration, the weak band in FT-IR range is allocated to OH at 1147

cm$^{-1}$. A good alignment with reported spectrum explains the theoretical measured 1184cm$^{-1}$ value by B3LYP process.

Bending mode of the O-H off-plan in the area 517-710 cm$^{-1}$[26] is at a higher incidence than in free O-H in intermolecular and intramolecular associations. In our present study, an O-H out-of-plane bending vibration is allocated in the FT-IR range at 551 cm$^{-1}$, the theoretically measured HF and B3LYP value also explains the same vibration form in the area 684 and 580 cm$^{-1}$ is assigned to O-H out-of- plane vibration.

### 5.2.3. C-H vibrations

The GPS fragment results in C-H stretching and C-H bending movements in the plane and C-H out of the plane. The C-H extending vibration is the key feature for identifying a C-heavily vibration in the area 2850-3000 cm-1, based on the literature analysis [27]. The anticipated C-H vibration is equal to the expanding modes (Mode No. 7-11) for the particle number. The Vibrational Mode nos (7-11), which are calculated with the 2997,2975,2969,2917,2873 and 2862 cm$^{-1}$, are allocated to glyphosine stretching mode C-H computed with the FT-IR spectral recording at 2646, the FT-Raman spectral at 3012, and the FT-Raman spectral at 2967cm$^{-1}$, respectively. In the 2990-2861 cm$^{-1}$ range, the same vibration degree of HF/6-31 G (d, p) calculated corresponds to the preliminary vibration.

In the area 1350-1470 cm$^{-1}$ is observed the C-H bending vibrations of alkanes and their plagiarism. The bands are sharp, but low to medium. A good deal of spectral compatibility with FT-IR is demonstrated by the 1477-1463 C-H bending vibrations measured HF and 1435-1306 cm$^{-1}$ by B3LYP/6-31 G (d) (d.p.). The same HF and B3LYP vibrations are also well consistent with provisional results. The theoretically developed C-H vibrations that stretch and bend are in good agreement with provisional values.

### 5.2.4. COOH vibrations

The extended band of carboxylic acids in the 1705-1720 cm$^{-1}$ range was generally observed. The band is induced by C = O vibration stretching. The double bond carbon oxygen is made by carbon and oxygen, because carbon and oxygen atoms have different electrical negativities. The single pair of oxygen electrons also decides about the character of the carbonyl group [28].In such cases, two C = O are predicted, one of which is Raman active in the process (symmetric delaying of vibrations) and another of which is IR active in the segment (anti-symmetric delaying of caress) [29]. Due to hydrogen bonding in the next-door group – COOH – most carboxylic acids in their solid state form dimeric composition. In our current analysis, C = O stretching vibrations with strong concordance with the HF / B3LYP/6-31 G (d, p) value of the worked-out value at 1812/756 cm$^{-1}$ are assigned a powerful stripe observed in FT-IR spectrums of 1722 cm$^{-1}$ and FT-Raman spectrums of 1734 cm$^{-1}$. In the region 1395-1440 cm$^{-1}$, the characteristic carboxylic group C = O is expected to vibrate, according to whether the species are monomeric, dimeric and other hydrogen bound. In the theoretical calculations the C = O bending vibration is assigned to 1437 and 1378 cm$^{-1}$ by FT-Raman, according to the HF method, and with 1367 and 1319 cm$^{-1}$ by the B3LYP method.

### 5.2.5. HCH and HCN bending

Vibrations of HCH and HCN bend and separate vibrations of NH2 and CH2 groups from twisting and scissors [30]. HCH vible vibration waves with HF and the B3LYP system values 1477,1469,1463cm$^{-1}$ and 1435,1415,1396cm$^{-1}$ in the FT-IR range at 1495, 1464 and 1394 cm$^{-1}$ and 1437 cm$^{-1}$ in the FT-IR spectrum. The scaled HF and DFT / B3LYP methods for the HCN vibrations are formed in 1359, 1343 and 1312 cm$^{-1}$ and 1311, 1283 and 1267 cm$^{-1}$wavenumbers.

### 5.2.6.Phosphorous group vibration

For Phosphorous functional group (P-OH) usually FT-IR region band is 1040-930 cm$^{-1}$[31]. Detailed wave number of the named P-OH fragments for HF and 1001.979, 970 and956 cm$^{-1}$ of the DFT / B3LYP process is 1111, 1025, 1019 and 987 cm$^{-1}$. In our case, P-OH stretching mode in FT-Raman coincides theoretically with a high band with 1049 cm$^{-1}$ and an FT-IR with a high 955 cm$^{-1}$.

The P = O-Stretching Mode for Phosphoramide and Phosphate-1 1200-1100 cm$^{-1}$ and Plagiarist [32] is allocated in area 1200-1275 cm$^{-1}$. In this case, the P = O stretch mode in FT-IR at 1238 cm$^{-1}$ is assigned as a band. The values for HF and DFT / B3LYP correspond with theoretical findings at 1264 cm$^{-1}$, 1228 cm$^{-1}$. For lipids, P-O asymmetrical deformation mode is 820 cm$^{-1}$[33].

The P-O asymmetrical stretch mode is available at 842 cm-1 in the titled fragment, while the theoretically anticipated wave numerals for the HF and DFT / B3LYP system are 861-841cm-1 and 810-784 cm$^{-1}$. In the waven numbers 420,403 and 388cm$^{-1}$ for the HF-method and for 365,363 and 349 cm$^{-1}$ for the DFT / B3LYp method, the FT-Raman spectrum is assigned to P-O bending mode.

*Table 4. Vibrational wave numbers obtained for Glyphosine at HF and B3LYP/6-31G (d, p) [harmonic frequency ($cm^{-1}$)].*

| Mode nos. | Experimental ($cm^{-1}$) | | Wave number ($cm^{-1}$) | | | | PED(%) |
|---|---|---|---|---|---|---|---|
| | FT-IR | FT-Raman | HF/6-31G(d,p) | IR $_{int}$ | B3LYP/6-31G(d,p) | IR $_{int}$ | |
| 1 | 3679w | | 3682 | 216.36 | 3686 | 135.36 | ν-OH (100) |
| 2 | 3615m | | 3680 | 204.02 | 3676 | 133.84 | ν-OH (99) |
| 3 | | | 3645 | 139.92 | 3658 | 140.79 | ν-OH (99) |
| 4 | | | 3512 | 527.64 | 3612 | 83.67 | ν-OH (100) |
| 5 | 3490m | | 3373 | 724.17 | 3499 | 468.95 | ν-OH (100) |
| 6 | | 3012vs | 2990 | 1.85 | 2997 | 2.15 | ν-CH (95) |
| 7 | | 2967vs | 2960 | 13.76 | 2975 | 4.21 | ν-CH (14)+ ν-CH (15)+ ν-CH (68) |
| 8 | 2946w | | 2951 | 8.68 | 2969 | 1.07 | ν-CH (27) + ν-CH (44) + ν-CH (27) |
| 9 | | | 2919 | 31.15 | 2917 | 15.71 | ν- CH (58) + ν-CH (41) |
| 10 | 2868vs | | 2912 | 11.57 | 2873 | 56.83 | ν-CH (95) |
| 11 | | | 2861 | 41.08 | 2862 | 31.52 | ν-CH (95) |
| 12 | 1722vs | 1734vs | 1812 | 400.00 | 1756 | 277.51 | ν-OC (86) |
| 13 | 1495w | | 1477 | 18.92 | 1435 | 9.36 | T- HCCO (11) + β -HCH (73) |
| 14 | 1464m | | 1469 | 12.44 | 1415 | 18.96 | β -HCH (18) +  β - HCH (54) |
| 15 | 1394m | | 1463 | 11.58 | 1396 | 0.84 | β -HCH (64) +  β -HCH (19) |
| 16 | | 1437s | 1436 | 39.18 | 1367 | 28.52 | ν-OC  (10) + ν-CC (11) +  ω - HCCO (21) |
| 17 | | 1378w | 1381 | 9.47 | 1319 | 46.41 | ν-OC (13) |
| 18 | | | 1359 | 14.16 | 1311 | 9.67 | ω - HCNC (24) + ω -HCNC  (27) |
| 19 | | | 1343 | 52.87 | 1293 | 16.34 | δ  -HCNC (16) + T-HCNC (30) +  γ -HCH (13) |
| 20 | | 1300m | 1312 | 46.55 | 1267 | 2.01 | ω -HCNC (17)+  ρ -HCNC (15) +  γ -HCN (31) |
| 21 | | | 1288 | 133.60 | 1249 | 40.89 | ν-PO (14) + γ  - HCN (25) +  β -HCC (24) |
| 22 | 1238m | | 1264 | 195.52 | 1228 | 164.68 | ν- PO (64) +  γ - HCN (12) |

*Table 4. ( Cond.)*

| Mode nos. | Experimental (cm⁻¹) | | Wave number (cm⁻¹) | | | | PED (%) |
|---|---|---|---|---|---|---|---|
| | **FT-IR** | **FT-Raman** | **HF/6-31G(d,p)** | **IR $_{int}$** | **B3LYP/6-31G(d,p)** | **IR $_{int}$** | |
| 23 | | 1243w | 1242 | 206.27 | 1222 | 293.88 | ν-PO (64) + β - HCN (14) |
| 24 | | | 1221 | 187.02 | 1204 | 29.11 | β -HOC (11) + β -HCC (13) |
| 25 | 1147w | | 1209 | 107.32 | 1154 | 126.24 | ν- OC (21) + β -HOC (24) |
| 26 | | 1173s | 1167 | 247.94 | 1095 | 90.76 | ν-NC (21) + ν-NC (20) |
| 27 | | | 1152 | 143.25 | 1084 | 109.96 | γ - HOP (73) |
| 28 | | 1123vs | 1119 | 109.65 | 1081 | 14.80 | ν-NC (37) + β - HCN (10) |
| 29 | | 1049s | 1111 | 61.81 | 1001 | 31.16 | β -HOP (66) |
| 30 | 955m | | 1025 | 85.25 | 979 | 50.10 | β - HOP (81) |
| 31 | | | 1019 | 70.30 | 970 | 64.85 | γ -HOP (14) + ρ – HCCO (17) |
| 32 | | | 987 | 14.23 | 956 | 44.44 | γ -HOP (58) |
| 33 | | 965w | 952 | 316.01 | 889 | 182.90 | ν-PO (15) + S-PO (22) |
| 34 | | | 941 | 264.62 | 879 | 188.72 | ν-PO (34) |
| 35 | | 927m | 905 | 46.23 | 857 | 51.32 | ν-OC (18)+ ν-CC (28) + ν- PO (12) |
| 36 | | | 889 | 116.99 | 850 | 74.76 | ω -HCNC (11) +ν-PO(28) |
| 37 | | | 884 | 33.95 | 832 | 45.43 | ν-NC (20) + ν-NC (12) |
| 38 | | | 861 | 280.57 | 810 | 328.28 | ν-PO (42) |
| 39 | | | 854 | 64.85 | 806 | 37.61 | ν-PO (38) |
| 40 | | 842w | 841 | 35.53 | 784 | 22.22 | ν- PO (42) + ν-PO (14) |
| 41 | 724w | | 748 | 42.56 | 720 | 52.15 | γ -OCOC (27) + γ - OCO (10) |
| 42 | | 725vs | 731 | 29.33 | 701 | 12.10 | β -PCN (10) + ν-PC(37) |
| 43 | 666w | | 710 | 60.32 | 678 | 26.21 | ν-PO (17) + ν-PC (34)+ ν-PC(11) |
| 44 | 551m | | 684 | 213.18 | 580 | 222.71 | ω -HOPC (67) |
| 45 | | 664w | 684 | 213.18 | 570 | 0.58 | ω -HOPC (18) + β - OCO (42) |
| 46 | | | 642 | 97.48 | 517 | 102.98 | τ - HOCC (64) |
| 47 | | 605w | 607 | 282.75 | 482 | 40.95 | γ -OCOP (25) |
| 48 | | | 561 | 41.51 | 457 | 44.53 | β -OPO(12)+ β –OPO(13)+ β – OPO(14) |

*Table 4. (Cond.).*

| Mode nos. | Experimental (cm$^{-1}$) | | Wave number (cm$^{-1}$) | | | | PED (%) |
|---|---|---|---|---|---|---|---|
| | FT-IR | FT-Raman | HF/6-31G(d,p) | IR $_{int}$ | B3LYP/6-31G(d,p) | IR $_{int}$ | |
| 49 | | 508w | 495 | 113.65 | 431 | 67.01 | τ -HOCC (13) + β -CNC (25) |
| 50 | | | 491 | 78.12 | 418 | 41.06 | T-HOPC (17) + γ -OPO (22) + γ OPO (18) |
| 51 | | 467vs | 452 | 19.31 | 412 | 14.92 | ω -HCCO (11) + β -OCC (49) |
| 52 | | | 437 | 4.46 | 392 | 22.16 | β - OPO(11) + β - OPO (33)+ β - OPO (10) |
| 53 | | | 420 | 103.87 | 376 | 5.42 | γ -OPO (27) + ω -HOPC (10) + γ -OPO (27) |
| 54 | | 400s | 403 | 43.30 | 365 | 59.35 | γ -OPO (36) + γ -OPO (10) |
| 55 | | | 388 | 21.13 | 363 | 36.34 | γ -OPO (11) + γ –OPO(34) + γ -OPO (19) |
| 56 | | | 375 | 22.48 | 349 | 120.32 | γ -OCOP (11) + ω -HOPC (49) |
| 57 | | | 333 | 2.62 | 306 | 6.33 | γ –CNC(35) |
| 58 | | | 331 | 9.15 | 279 | 3.10 | ω -PCNC (10) + γ –OCOP(13)+ γ -CCCN (15) |
| 59 | | | 296 | 8.35 | 267 | 33.22 | γ -OCOP (11) + τ -HOPC (13) |
| 60 | | | 277 | 5.87 | 224 | 18.67 | γ -OCOP (17) + τ – HOPC(30) |
| 61 | | | 241 | 13.59 | 215 | 13.58 | γ –OCOP(17) + β -CNC (13) |
| 62 | | | 223 | 25.09 | 192 | 33.66 | β -OPO (18) + τ -HOPC (24) |
| 63 | | | 181 | 90.79 | 157 | 5.11 | γ –OCOP(10) + β -PCN (29) |
| 64 | | | 175 | 17.55 | 144 | 3.74 | γ-OCOP (21)+ γ -PCN (34) |
| 65 | | | 168 | 86.33 | 141 | 43.39 | ω - OPCN (24) + ω-OPCN (12) + ω -HOPC (23) |
| 66 | | | 147 | 0.57 | 118 | 26.34 | δ -PCNC (33) |
| 67 | | | 144 | 3.27 | 92 | 23.04 | δ -PCNC (21)+ ω -HOPC (22) + β -OPO (10) |
| 68 | | | 133 | 0.70 | 80 | 3.66 | δ -OCCN (31) + τ -CCNC (21) + ω –OPCN(16) |
| 69 | | | 101 | 4.83 | 61 | 1.18 | ω-OPCN(18)+ γ -CCCN (11) + β-CNC (10) |
| 70 | | | 79 | 2.57 | 48 | 6.73 | δ -OPCN (20) + ω -PCNC (24) |
| 71 | | | 57 | 1.23 | 39 | 0.81 | δ -CCNC (44) + ρ-PCNC(25) |
| 72 | | | 42 | 1.91 | 34 | 0.70 | δ-OCCN (19) + τ-OPCN (32)+ τ -OPCN (20) |

IR $_{int}$ -IR intensity; Kmmol$^{-1}$w-weak ; vw- very weak ; s-strong ; vs-very strong ; m-medium; υ - stretching; β- in plane bending ;     γ- out-of –plane bending ; ω – wagging ; t- twisting ; δ –scissoring ; τ- torsion.

## 6. HOMOand LUMO analysis

These orbits are the brace that is most closely associated with the energy of any pair of orbital fragments [34]. The intramolecular reassignment of the contributor to the assembly by a double-to-one-bond conjugated route will induce broad variations of molecular jiffy dipole and molecular polarization in order to enhance IR and Raman behavior simultaneously. The relative intensities from electron cloud movement through the conjugated frames of an electron donor to an electron acceptor group in Raman and in IR spectrums are also found in FT-IR glyphosine bands that have their complements in Raman. The preliminary spectrum is well defined by the initial calculations in conjugated systems which predict extraordinarily high Raman and infrared intensities in the same normal modes [35, 36]. The wave function study indicates that electron absorption corresponds to the transition from the ground into the first keyed-up state and is determined primarily from the highest occupied molecular orbital ( HOMO) to the lowest unoccupied molecular orbital ( LUMO).
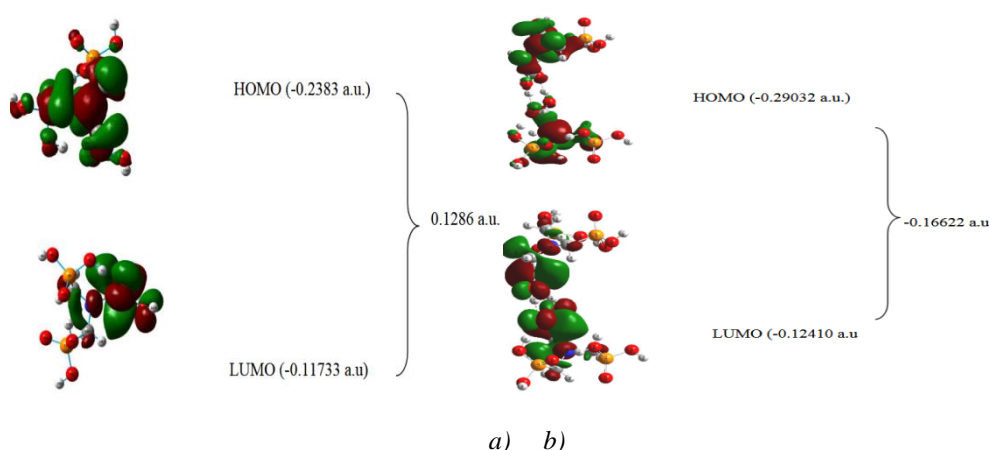


HOMO (-0.2383 a.u.)

0.1286 a.u.

LUMO (-0.11733 a.u)

HOMO (-0.29032 a.u.)

-0.16622 a.u

LUMO (-0.12410 a.u

a)    b)

*Fig. 7a.Compositions of the frontier molecular orbital forGlyphosine.*
*a) monomer atomic orbital*
*b)dimer atomic orbital*

The energy divide of GPS from HOMO-LUMO has been worked out at level B3LYP/6-31 (d, p) and shows (fig. 7) that the difference in energy is indicative of the fragment's chemical activity (Table 5). LUMO's ability to get an electron is symbolic of HOMO's ability to contribute an electron. Titled fragments are formed in the DFT / B3LYP/6-31 (d, p) level at the dimer HOMO-LUMO energy gap as shown in (Fig. 8). The energy difference of the GPS fragment dimer is greater than the GPS fragment monomer. The self-compatible GPS energy field (SCF) is -1498.474 a.u. In fact, the lower energy difference between HOMO and LUMO describes the subsequent transition of charges within the fragment. The orbital's in the border region that display virtually degenerated energy.
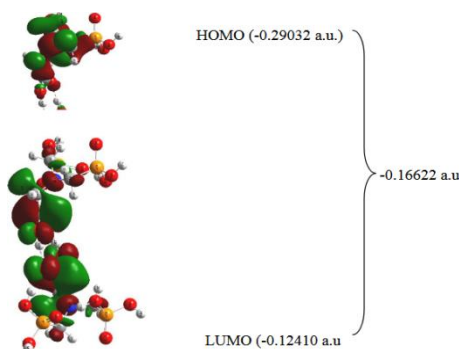
*Fig. 8. The dimer atomic orbital compositions of the frontier molecular orbital for Glyphosine.*

The Multiwfn study included complete state densities (TDOS), partial state density (PDOS) and partial overlay of states density (OPDOS) [37, 38]. The pictures of the state density show that energy of the functional group and the glyphosine energy element is within the range of -1.0 a.u. 6.0 a.u. A.u. In (Figure 9) showed. From the imagery of the homo-light-marked line overlapped with the density of states N, C-C and the hydroxyl group of the fragment named. The pictorial representation of the nitrogen and OH density distribution group is overlaid to the GPS fragments' homo-lump energy difference.

*Table 5. HOMO-LUMO energy value calculated by HF/B3LYP/6- 31G (d, p) method for monomer and dimer of Glyphosine.*

| Parameters | Monomer | dimer |
|---|---|---|
| | B3LYP/6-31G(d,p) | B3LYP/6-31G(d,p) |
| HOMO (a.u) | -0.38646 | -0.29032 |
| LUMO(a.u) | -0.11733 | -0.12410 |
| HOMO-LUMO(a.u) | -0.26913 | -0.16622 |

## 7. Potential energy surface scans

Figures 10a and 10b. 10a and 10b display the possible surface scan for the title fragment with the B3LYP/6-31 G (d, p) degree of theoretical approximation. The C11-C14-O15-H16 dihedral angle for GPS provides the appropriate co-ordinate for the elasticity of conformation of the fragments. The geometrical hops were all simultaneously loosened by B3LYP/6-31 G (d, p) measurement, while the torsional angle C11-C14-O15-H16 in 10o steps varied 10° to 360°. While for the dihedral angle of C11-C14-O15-H16, the maxima of the future energy curve at 190 ° (-1498.75529 Hatree), appears in 100° and 280°. The minimum total (– 1498.74429 and -1498.74351 Hatree for the 280°) is probable due to the fact that methoxy and other hydrogen present in the fragment at this angle is not influenced by this hydroxy group. The C2-P5-O6-H9 dihedral angle was varied from 0° to 360° in 10° stage for named fragments. The prospective energy curve of two maxima and one minimum was observed. The C2 P5 O6-H9 average forward energy for scans is -1498.4814 for 40 degrees and -1498.4807 for 360 degrees and the lowest prospective scanning energy is -1498.4727 for 230 degrees. For dihedral angles (C11-C14-O25-H16 and C2-P5-O6-H9), the highest and lowest prospective scanning energy for the GPS fragments is present but prospective energy is not very varying because C-C and C-P will cause both dihedral angles.
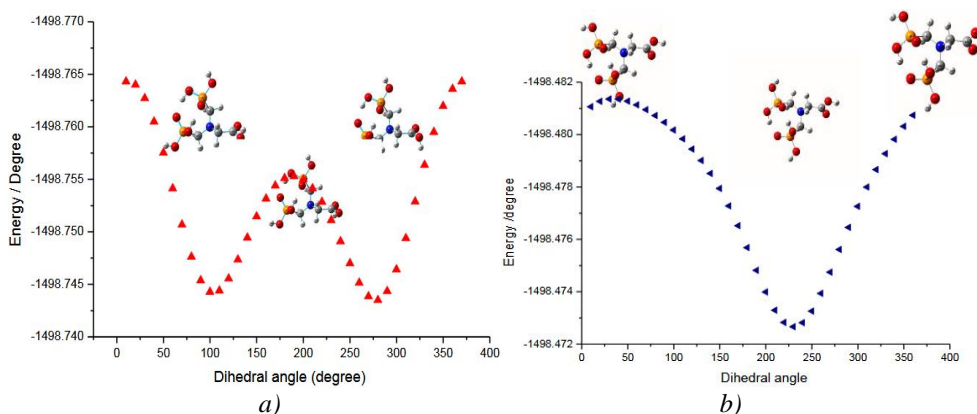
*a)*          *b)*

*Fig. 10a.PES scan for dihedral angle*
*a) C11-C14-O15-H16 at b3lyp/6-31(d,p).*
*b) C2-P5-O6-H9 at b3lyp/6-31(d,p).*

## 8. Thermodynamic properties

The theoretical method shown in Table 6 was used to perform statically thermodynamic functions such as a specific heat capacity, heat capacity and entropy changes with varying temperature from 100 to 1000 Kk. Based on the vibratory analysis, this thermodynamic hops can be observed as the temperature increases [39]. The corresponding correlation graph (Figure 11) of thermodynamic functions follows

$$S = 215.32 + 0.2973\,T - 1.2 \times 10^{-4}T^2$$

$$C_p = 28.98 + 0.140\,T - 7.6 \times 10^{-5}T^2$$

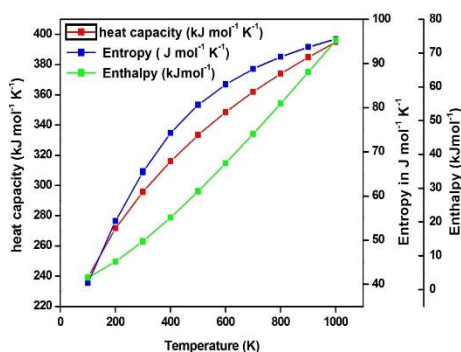$$\Delta H = -2.523 + 0.049\,T + 2.7 \times 10^{-5}T^2$$



*Fig. 11. Correlation graphic of heat capacity, entropy and enthalpy versus temperature for Glyphosine.*

*Table 6. Thermodynamic properties at different temperatures for Glyphosine.*

| T (K) | S (J/mol.K) | Cp (J/mol.K) | ΔH (kJ/mol) |
|-------|-------------|--------------|-------------|
| 100 | 311.48 | 87.59 | 5.35 |
| 200 | 394.69 | 158.69 | 17.77 |
| 298 | 469.51 | 218.43 | 36.35 |
| 300 | 470.86 | 219.46 | 36.76 |
| 400 | 541.09 | 269.2 | 61.29 |
| 500 | 605.51 | 308.01 | 90.23 |
| 600 | 664.45 | 338.16 | 122.6 |
| 700 | 718.44 | 362.13 | 157.66 |
| 800 | 768.12 | 381.74 | 194.88 |
| 900 | 814.05 | 398.2 | 233.9 |
| 1000 | 856.76 | 412.26 | 274.44 |

## 9. Natural bonding analysis

The bonding NBOs come from the orbital Lewis and the non-Lewis orbital antibonding NBOs. The complete Lewis orbital's are complemented by officially vacant non-Lewi orbital's with an idealized Lewis structure. The lower electronic load in Lewis orbital's shows good electron relocation effects. The Analysis of the NBO provides more information about the communication between empty and filled orbit which could improve intramolecular communication analysis. For each NBO donor NBO (i) and accepter NBO (j) the Fock analysis perturbation theory is estimated for the second order: the delocation (2e-stabilization) "energy stabilization energy E(2) is estimated at [40,41].

$$E(2) = \Delta E_{ij} = q_i \frac{F(i,j)^2}{\varepsilon_j - \varepsilon_i} \tag{9}$$

The E(2) value for electron donor and electron acceptor communication is higher, and value is higher. An NBO study is performed by means of a named B3LYP fragment for the divulgation of electron density into fragments intramolecular, rehybridizationand delocation [42, 43]. The Oxygen-Lone bonding pair and C-O antibonding pairs = 46.18 and 31.78 kcal / mol are recorded for the strongly stabilizing contact of σO23 →σ*C10-O11 and σO11 →σ*C10-O23. An interaction between the O to C-O bond orbit forms the intramolecular hyper conjugate contact that results in the contact charge transfer that results in the stabilization within the fragment as well as in the results shown (Table 7).

*Table 7. Second order perturbation theory analysis of Fock matrix in NBO basis*
*for Glyphosine molecule.*

| Donor NBO (i) | TYPE | ED/e | Acceptor NBO (j) | Type | ED/e | E(2) kcal/mol | E(j)-E(i) | F(i,j) |
|---|---|---|---|---|---|---|---|---|
| P 5 - O 19 | σ | 1.98548 | P5 - O21 | σ* | 0.17439 | 3.34 | 1.05 | 0.055 |
| C 7 - H 8 | σ | 1.98636 | C10 - O23 | σ* | 0.09654 | 3.53 | 0.89 | 0.051 |
| C 7 - H 9 | σ | 1.97158 | N 1 - C12 | σ* | 0.02228 | 4.59 | 0.84 | 0.056 |
| C 7 - C 10 | σ | 1.97849 | N 1 - C2 | σ* | 0.02371 | 3.37 | 0.98 | 0.051 |
| C 12 - H 14 | σ | 1.98532 | N 1 - C2 | σ* | 0.02371 | 2.78 | 0.87 | 0.044 |
| C 12 - P 15 | σ | 1.96847 | P15 - O25 | σ* | 0.16233 | 3.63 | 0.82 | 0.05 |
| P 15 - O 25 | σ | 1.98713 | P 15 - O 17 σ* | | 0.16233 | 3.14 | 1.06 | 0.054 |
| O 23 - H 24 | σ | 1.98364 | C 7 - C10 | σ* | 0.06850 | 4.09 | 1.09 | 0.061 |
| O 6 | π | 1.99981 | P 5 | π* | 0.02618 | 3.32 | 19.55 | 0.229 |
| O 11 | π | 1.99973 | C10 | π* | 0.02084 | 7.26 | 19.68 | 0.339 |
| O 16 | π | 1.99973 | P 15 | π* | 0.05576 | 3.51 | 19.59 | 0.236 |
| N 1 | σ | 1.99937 | C 7 - H 8 | σ* | 0.0694 | 7.66 | 0.68 | 0.066 |
| O 6 | σ | 1.97993 | P 5 - O 21 | σ* | 0.17439 | 24.95 | 0.48 | 0.099 |
| O 11 | σ | 1.97686 | C10 - O 23 | σ* | 0.09654 | 31.78 | 0.63 | 0.128 |
| O 16 | σ | 1.97869 | P15 - O17 | σ* | 0.16233 | 25.48 | 0.48 | 0.1 |
| O 17 | σ | 1.92561 | P15 - O25 | σ* | 0.16979 | 10.17 | 0.58 | 0.07 |
| O 21 | σ | 1.96412 | P 5 - O19 | σ* | 0.18525 | 10.21 | 0.54 | 0.068 |
| O 23 | σ | 1.91208 | C10 - O11 | σ* | 0.02263 | 46.18 | 0.34 | 0.113 |
| O 25 | σ | 1.96178 | P 15 - O 16 σ* | | 0.07503 | 8.08 | 0.72 | 0.068 |
| P 5 - O 21 | π | 1.98707 | P 5 | π* | 0.05798 | 12.14 | 0.53 | 0.211 |
| P 15 - O 25 | π | 1.98713 | P 15 | π* | 0.05576 | 12.83 | 0.53 | 0.219 |

## 10. Mulliken charges

The application of quantum mechanical calculation to molecular system [44] is a critical atomic charge feature. The electrical charge of each atom is based upon the fragment's ability to bind. HF and B3LYP/6- 31 G (d, p) method are used to evaluate the mulliken atomic charge of the GPS fragment. The GPS fragment's total



*Fig. 12. Comparative of Mulliken's plot based on HF / B3LYP / 6-31G (d, p) method for Glyphosine.*

Charges are (Fig. 12). It is evident from Table 8 that the P substitute of the fragment results in a higher electron density than the other alternating atoms. In the GPS fragment for HF and DFT / B3LYP process, the Mulliken atomic charge of the O atom gets more negative.

## 11. Conclusions

The frequency assignment for the GPS was carried out by FTIR and FT-Raman. On the theory level ab initio HF and DFT, the balancing geometries and harmonic GPS frequencies were defined and analyzed. The fact that the computations were made in the gaseous state with a single fragment, as opposed to the timely values recorded in the presence of intermolecular contact, may result from any observed divergence and the measured frequencies. There is a very small difference between the observed and the scaled values of wave numbers in many basic concepts.

Consequently, the tasks at DFT theoretical level tend to be accurate even with reasonable deviations from the provisional values. The FT-IR spectrum constructed theoretically coincides with the tentatively observed FT-IR spectrum. The DFT theory has drawn up two separate forward-looking energy scans for the hydroxy group called the fragment. The HF-method with 6-31 G (d, p) base set has worked out the electrical dipolar moments and first hyperpolarizability of the studied composite. The GPS fragment was analyzed on HOMO-LUMO energy and density distribution. The DFT / B3LYP system was used to perform the NBO analysis of Glyphosine. The energy of stabilization was examined by DFT method of natural bonding. This study shows that DFT / B3LYP calculations are a strong way of interpreting organic composite vibrations.

## References

[1] S.M. Croft, C.J. Arntzen, L.N. Vanderhoef, C.S.Zettinger,BiochimicaetBiophysica Acta (BBA)-Nucleic Acids and Protein Synthesis**335**,211(1974).
[2] A. Hershman, W. Knox, F. Paulik, J. Roth, (1973), U.S. Patent No 3,769,329. Washington, DC: U.S. Patent and Trademark Office.
[3] A. Lehuen, J. Diana, P. Zaccone, A. Cooke, Nature Reviews Immunology**10**,501(2010).
[4] A. Samsel, S.Seneff, Interdiscip. Toxicol.**6**,159 (2013).
[5] G.M. Williams, R. Kroes, I.C. Munro, Regul.Toxicol. Pharm.**31**,117(2000).
[6] A. Samsel, S. Seneff, Entropy **15**,1416(2013).
[7] N. De María, J.M. Becerril, J.I. García-Plazaola, A. Hernández, M.R. de Felipe, M. Fernández-Pascual, J. Agr. Food Chem. **54**,2621(2006).
[8] J. E. Franz, M. K. Mao, J. A. Sikorski, ACS Monograph **189**, 653 (1997).
[9] M. Malven, J. Rinehart, N. Taylor, E. Dickinson (2009), US Patent No 7,632,985, Washington, DC: U.S. Patent and Trademark Office.
[10] T. Senapati, A.K. Mukerjee, A.R. Ghosh, J. Crop Weed**5**,236(2009).
[11] C. Hershko, J. Patz, Haematologica **93**,1761 (2008).
[12] A. Samsel, S. Seneff, Interdiscip. Toxicol.**6**,159 (2013).
[13] R.E. Hoagland (1980), Effects of glyphosate on metabolism of phenolic compounds: VI. Effects of glyphosine and glyphosate metabolites on phenylalanine ammonia-lyase activity, growth, and protein, chlorophyll, and anthocyanin levels in soybean (Glycine max) seedlings, Weed Science, 393-400.
[14] L.F. Kubena, H.E. Smalley, F.M.Farr, Poul.Sci. J.**60**,132 (1981).
[15] M. J. Frisch et al., Gaussian 09, revision A, 1 Gaussian Inc., Wallingford C T.
[16] H.B. Schlegel, J. Comp. Chem. **3**, 214 (1982).
[17] R. Dennington, T. Keith, J. Millam, (2009), Gauss View, version 5, Semichem Inc., Shawnee Mission K S.
[18] M.H. Jamróz, Spectrochim. Acta Part A: Mol. Biomol. Spectrosc.**114**,220 (2013).
[19] D.A. Kleinman, Phys. Rev. **126**,1977 (1962).[20] P. Pulay, G. Fogarasi, G. Pongor, J.E. Boggs, A. Vargha, J. Am. Chem. Soc. **105**,

7037 (1983).

[21] M. Samsonowicz, T. Hrynaszkiewicz, R. Świsłocka, E. Regulska&W. Lewandowski, J. Mol.Struct.**744**,345 (2005).

[22] M. Amalanathan, V.K. Rastogi, I.H. Joe, M.A.Palafox, R. Tomar, Spectrochim. Acta Part A: Mol. Biomol.Spectrosc.**78**,1437 (2011).

[23] D. Sajan, H. Joe, V.S. Jayakumar, J. Zaleski, J. Mol.Struct. **785**, 43 (2006).

[24] D. Michalska, D.C. Bienko, A.J. Abkowicz-Bienko, Z. Latajka, J. Phys. Chem. **100**, 17786 (1996).

[25] G. Varsányi (1974), Assignments for vibrational spectra of seven hundred benzene derivatives (Vol. 1), Halsted Press.

[26] D.N. Sathyanarayana (2015), Vibrational spectroscopy: theory and applications, New Age International.

[27] H.J. Geise, H.R. Buys, F.C. Mijlhoff, J. Mol.Struct. **9**,447(1971).

[28] N.M. Brown, R.J. Turner, D.G. Walmsley, Journal of the Chemical Society, Faraday Transactions 1: Physical Chemistry in Condensed Phases **77**,2481 (1981).

[29] T. Miyazawa, T. Shimanouchi, S.I. Mizushima, J. Chem. Phys. **29**,611 (1958).

[30] M.M. Schiavoni, H.G. Mack, S.E. Ulic, C.O. Della Vedova, Spectrochim. Acta Part A: Mol. Biomol. Spectrosc.**56**,1533 (2000).

[31] Y. Zheng, J. Dong, B.A. Palfey, P.R. Carey, Biochem. **38**, 16727 (1999).

[32] A.M. Abuelela, T.A. Mohamed, O.V. Prezhdo,J. Phys. Chem. C**116**, 14674 (2012).

[33] C. Wang, K.M. Durney, G. Fomovsky, G.A. Ateshian, S. Vukelic(2016, March), In SPIE BiOS (pp. 970415-970415), International Society for Optics and Photonics.

[34] F. De Proft, P. Geerlings, Chem.Rev. **101**,1451 (2001).

[35] B.Lakshmaiah, RamanaG.Rao, J. Raman Spectrosc.**20**. 439 (1989).

[36] M. Govindarajan, M. Karabacak, A. Suvitha, S. Periandy, Spectrochim. Acta Part A: Mol. Biomol.Spectrosc.**89**,137 (2012).

[37] J.A. Sañudo-Barajas, J. Labavitch, C. Greve, T, Osuna-Enciso, D.Muy-Rangel, J. Siller-Cepeda, Postharvest Biol. Technol. **51**,158 (2009).

[38] Lu Tian, Feiwu Chen, J. Comp. Chem. **33**,580 (2012).

[39] L. Sinha,O. Prasad, S. Chand, A.K. Sachan, S.K. Pathak, V.K. Shukla, M. Karabacak, A.M. Asiri, Spectrochim.ActaPart A Mol.Biomol. Spectrosc.**133**,165 (2014).

[40] ShahriarGhammamy, Amir Lashgari, Middle East J. Sci. Res.**17**,1080 (2012).

[41] A.E. Reed, F.Weinhold, J. Chem. Phys. **78**, 4066 (1983).

[42] A.Srivastava, Ambrish Kumar, NeerajMisra, J. Fluorine Chem. **158**,65 (2014).

[43] N. Prabavathi, A. Nilufer, V.Krishnakumar, Spectrochim. Acta Part A: Mol. Biomol. Spectrosc. **92**,325 (2012).

[44] R.S. Mulliken, J. Chem. Phys. **23**,1833 (1955).